ELSEVIER

S0052-3861(96)00440-5

Polymer Vol. 37 No. 26, pp. 5769–5779, 1996

0032-3861/96/$15.00+0.00

polymer papers

Polarized light scattering studies on the orientational behaviour of liquid crystalline rods immersed in shear flow under the action of an electric rectangular pulse

Masaru Matsuo* and Maki Nakano
Department of Textile and Apparel Science, Faculty of Human Life and Environment, Nara Women's University, Nara 630, Japan

Tetsuya Ogita
Department of Materials Science and Engineering, Faculty of Engineering, Yamagata University, Yonezawa 992, Japan

and Mitsuhiro Matsumoto
Department of Chemistry, Faculty of General Science, Tokushima University, Tokushima 770, Japan
(Received 29 August 1995; revised 2 January 1996)

This paper deals with theoretical treatments for the deformation mechanism of liquid crystal rods by light scattering under H_v polarization condition, when the rods oriented by a shear flow are acted on by a rectangular electric pulse along the direction of the velocity gradient of flow. As in one example, the calculations were carried out to check whether the complicated orientational behaviour of superstructures such as rods and/or spherulites cause significant effect on the profile of H_v light scattering patterns. In the present system, the orientation distribution function of rods was obtained as the solution of the rotational diffusion equation for rotational ellipsoidal particles. In actual calculations for light scattering patterns, the orientational fluctuation with respect to the rod axis is considered to explain the circular type pattern under no external excitation which has been reported in previous experiments. When the orientation functions provide curves showing two peaks by the proper choice of parameters concerning electric field strength and velocity gradient, the corresponding H_v light scattering pattern showed four small dull lobes in the vertical direction indicating the preferential orientation of rods with respect to the shear flow direction in addition to the four sharp large lobes in the horizontal direction indicating the preferential orientation of rods with respect to the electric field direction. This indicates that the H_v light scattering pattern influences the two kinds of orientation of rods.

(Keywords: liquid crystal rods; light scattering; H_v polarization condition; shear flow; rectangular electric pulse)

INTRODUCTION

Small angle light scattering under polarization condition has been developed to study morphology of heterogeneous superstructures. The scattering patterns which have been most frequently found in the crystalline and liquid crystalline polymers are those from spherulitic[1] and rod-like textures[2]. The origin of the scattering has been shown to be mainly described by the analysis for H_v and V_v polarization conditions in terms of optically anisotropic spheres, or rods, since the patterns from both the superstructures are quite different to each other. The H_v scattering depends upon anisotropy of structures, while V_v scattering also depends upon density fluctuation, i.e. polarizabilities of the heterogeneous texture and of the surrounding medium. The V_v pattern is less distinct in comparison with the H_v pattern, reflecting the contribution to the density fluctuation. The typical light scattering from the heterogeneous system has been developed and is one of the most convenient and effective methods for studying the morphology because of the very short irradiation time of incident beam to a specimen usually less than 1 s[1–5]. Even so, however, light scattering patterns contain a more complicated factor concerning optical anisotropy in comparison with small angle X-ray scattering depending on only the electron density fluctuation. This indicates that the Fourier transfer of scattered intensity to obtain information on heterogeneous substances in a real space is meaningless.

Accordingly, theoretical calculations have been carried out to give the best fit between numerical and experimental results by selecting suitable values of the parameters associated with orientational fluctuation of optical axes and optical anisotropy. This method has played an important role in analysing the morphology of oriented and unoriented heterogeneous systems. The

* To whom correspondence should be addressed

theories for oriented polymer films by elongation have been formulated by using simple orientation distribution such as affine fashion[6,7]. For lyotropic liquid crystals, the orientation distribution of heterogeneous rods has been given as a function of time and applied electric field[8], since birefringent phase sometimes show rodlike and/or spherulitical textures under optical micrographs (crossed-polarized) and H_v polarization condition[9–14].

The theory of the liquid crystal system was based on electro-optical properties of rigid molecules such as polypeptides which can form liquid crystals in concentrated solutions as the molecular assembly. The investigation was developed in accordance with the concept that the electric anisotropy of a rigid molecule in a dilute solution causes the interaction energy of the molecule with the applied field to depend upon the angle between the molecular axis and the applied field[15,16]. O'konski *et al.* studied electrical and optical parameters from the saturation of the electric birefringence in a solution[16]. The saturation behaviour was computed for various ratios of permanent to induced moment contributions to the birefringence. The electrical parameters and the optical anisotropy factor of the molecules were separately determined by fitting the experimental birefringence saturation results to a theoretical curve. Since then, this treatment was extended to a disc-shaped particle by Shah[17,18] and to the more general molecular model by Holcomb and Tinoco[19]. As a further development based on the above concept, the orientation distribution function of macromolecule clusters was derived by the diffusion equation by Benoit[20] and Matsumoto *et al.*[21], in which the molecular axes are assumed to orient parallel to the molecular cluster axis (rod axis). By using this method, the time-dependence of the light scattering pattern was analysed when a rectangular pulse and a reversing pulse were applied to the nematic liquid crystalline solution by Matsuo *et al.*[22].

This paper is focused on the further theoretical analysis of scattered intensity from anisotropic liquid crystal rods with complicated orientational behaviour, since rodlike structures as an aggregation of rigid polymer chains were observed in the birefringent phase under optical micrographs (crossed-polarized) and H_v polarization condition[12–14]. As an example, the calculations were also carried out for time-dependence of the change in light scattering patterns when a rectangular pulse of an electric field strength was applied to nematic liquid crystal rods which had been oriented in the steady state flow direction perpendicular to the electric field. This system is much more complicated than the previous one with a random orientation of rods before the applied electric field. The rotational diffusion equation for rotational ellipsoidal particles in solution was approximately solved by one of the co-authors, Matsumoto[22], when the solute particles oriented by a shear flow were acted on by a rectangular and reversing electric pulse along the direction of the velocity gradient of flow. The angular distribution was obtained up to the fourth order for an electric field and/or hydrodynamic field and was applied to electric birefringence and extinction angle. As a further complicated application, H_v scattering patterns were calculated by assuming that the angular distribution obtained by the rotational diffusion equation is equal to that of the rod axis.

As discussed before, Fourier transfer of scattered intensity from heterogeneous substances is meaningless, since the scattered intensity depends on the complex relationship between an effective induced dipole moment of the scattering element depending upon the rotation of substances and phase retardation. Thus, any effective information from scattered intensity cannot be deduced without the comparison between observed pattern and the theoretical one calculated by using a proper model. The numerical results will probably offer useful information for the analysis of complicated orientation of rods exhibiting patterns with eight lobes[23,24]. Accordingly, the theoretical analysis for complicated systems, such as the simultaneously flow and electric orientation of rods, is of interest in understanding the application limit of the polarized light scattering technique to investigate complicated heterogeneous polymeric systems.

RESULTS AND DISCUSSION

It is well-known that molecules in liquid crystals orient parallel in the preferred direction[25]. This is usually one of the characteristics of liquid crystals in the case that the distance between two plate surfaces of the cell is thin and the concentration of solution is high[25]. The two factors depend on the types of chemical structure. According to our experimental results, however, it was confirmed that in addition to low molecular liquid crystals such as aqueous sodium dibutyl phosphate[26], the preferential orientation of rigid polymer chains can also be avoided by selecting two factors, concentration of solutions and thickness of a cell. Namely, the orientation of liquid crystal molecules in the preferred direction without applied external excitation could be avoided for poly(γ-bengyl-L-glutamate) (PBLG) in a chloroform system, the concentration being 11 vol% and the thickness being 200 μm. Thus, the following calculation will be carried out for the above system.

Figure 1 shows the schematic diagram which is necessary to calculate H_v scattered intensity from the rod of length L and infinitesimally thin diameter. The incident beam whose propagation direction is denoted by a unit vector $\mathbf{s}_0$ is detected as a function of θ, the

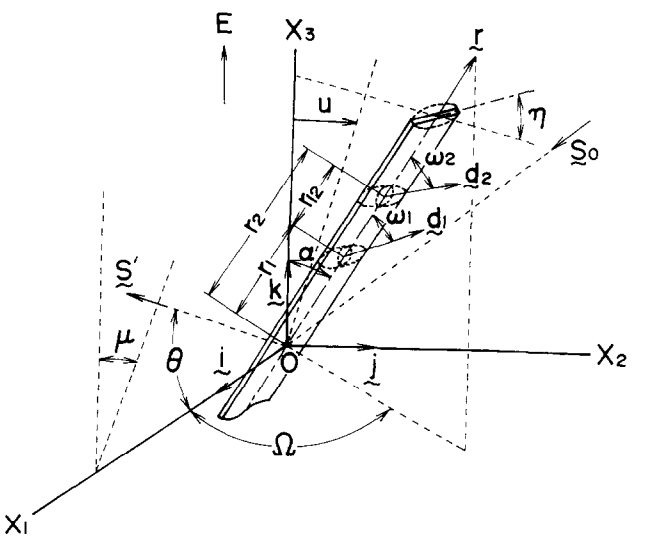

Figure 1 Schematic diagram showing the coordinate system of light scattering from the three-dimensional assembly of anisotropic rod under laminar flow and electric field

scattering angle, and μ, the azimuthal angle taken from the vertical direction OX_3 corresponding to an electric field direction. Before applying an electric field, the rod is oriented in the X_1 direction by the shear flow having a velocity vector **u**. Angles α and Ω are the polar and azimuthal angles of the rod with respect to Cartesian coordinate O–$X_1X_2X_3$ and angle η specifies the rotation angle of the rod around the vector **r** along the rod axis.

According to the Rayleigh–Gans theory[25], the amplitude A of the scattering from the rod may be given by

$$A = C\int_{-L/2}^{L/2}(\mathbf{M}\cdot\mathbf{O})\exp\{\mathrm{k}(\mathbf{r}\cdot\mathbf{s})\}\mathrm{d}\mathbf{r} \tag{1}$$

where C is a constant, and **s** is the scattering vector defined by $\mathbf{s_0} - \mathbf{s}'$, and k is given by $2\pi/\lambda'$, where λ' is the wavelength of light in the medium. The vector **M** is the dipole moment of the scattering element at r from the centre of the rod. The vector **O** is a unit vector along the polarization direction of the analyser set in between the specimen and the detector registering the scattering.

When an electric field is applied to the solution with steady-state flow, the scattered intensity I from a rod at time t may be given by

$$I = \frac{C\int_0^{2\pi}\int_0^{2\pi}\int_0^{\pi}F(\alpha,\Omega,t)AA^*\sin\alpha\,\mathrm{d}\alpha\,\mathrm{d}\Omega\,\mathrm{d}\eta}{\int_0^{2\pi}\int_0^{2\pi}\int_0^{\pi}F(\alpha,\Omega,t)\sin\alpha\,\mathrm{d}\alpha\,\mathrm{d}\Omega\,\mathrm{d}\eta} \tag{2}$$

where $F(\alpha, \Omega, t)$ is an orientation distribution function of a rod. In the absence of an electric field, $F(\alpha, \Omega, t)$ depends on the orientation of the rod immersed in a shear flow and is independent of t. A^* denotes a complex conjugate of A.

As shown in *Figure 1*, the orientation of optical axes with respect to the rod axis is dependent upon the position within a rod. This concept is introduced to explain a circular type pattern of H_v scattering from the PBLG–chloroform system under no external excitation. If the orientation of the optical axis of the scattering element ω fluctuates with r from their average value ω_0, ω is a function of r similar to $\omega(r) = \omega_0 + \Delta(r)$, where $\Delta(r)$ is the local fluctuation of ω. In this viewpoint, the angles ω_1 at r_1 and ω_2 at r_2 may be given by $\omega_1 = \omega_0 + \Delta_1$ and $\omega_2 = \omega_0 + \Delta_2$, respectively. When the difference between orientation fluctuation Δ_1 at r_1 and Δ_2 at r_2 is given by the quantity Δ_{12}, and defined by $\Delta_{12} = \Delta_2 - \Delta_1 = \omega_2 - \omega_1$, the angle characterizing the relative orientation of the optical axes of two scattering elements is separated by the distance, $r_{12} = r_1 - r_2$. The quality Δ_{12} has been related to the correlation function $f(r_{12})$ where

$$f(r_{12}) = \langle\cos 2\Delta_{12}\rangle_{\mathrm{av}} \tag{3}$$

The correlation function which, in general, decreases asymptotically from unity to zero with increasing distance $|r_{12}|$ from zero, is assumed to be given by the empirical function

$$f(r_{12}) = \exp(-|r_{12}|/c) \tag{4}$$

where c is the correlation distance. This method was first proposed in connection with the problem of an undeformed spherulite by Stein and Chu[28]. The parameter is expected to be related for a particular model of the fluctuating system, as discussed by Stein and Chu for the undeformed spherulite[28]. Obviously, the equation interrelating this parameter derived by Stein and Chu, can be used for the orientation fluctuation in a rod. This method was first employed by Hashimoto *et al.*[28] and the same procedure was used in the previous papers[11–14]. In these studies, $\langle\cos 2\Delta_1\rangle_{\mathrm{av}}$ and $\langle\cos^2 2\Delta_1\rangle_{\mathrm{av}}$ are given by

$$\langle\cos 2\Delta_1\rangle_{\mathrm{av}} = \frac{2}{(L/c)^2}[L/c - 1 + \exp(-L/c)] \tag{5}$$

$$\langle\cos^2 2\Delta_1\rangle_{\mathrm{av}} = \frac{1}{2} - \frac{1}{16(L/c)^2} \times [1 - 4(L/c) - \exp(-4L/c)] \tag{6}$$

Equation (4) reduces to zero as c approaches zero and to unity as c becomes large. On the other hand, equation (6) approaches 1/2 as c approaches zero, corresponding to completely random fluctuation. The quality approaches unity as c becomes large, corresponding to the absence of internal disorder. Incidentally, the effect of the orientational fluctuation must be introduced to the experimental results that the H_v pattern shows circular-type in the absence of the external applied field[13].

Based on the above concept, equation (2) can be rewritten as

$$I_{H_v} = C\int_0^{2\pi}\int_0^{\pi}\int_0^{L}F(\alpha,\Omega,t)(L - r_{12})\langle Q\rangle_\eta \times \cos Br_{12}\sin\alpha\mathrm{d}r_{12}\mathrm{d}\alpha\,\mathrm{d}\Omega \div \int_0^{2\pi}\int_0^{\pi}F(\alpha,\Omega,t)\sin\alpha\,\mathrm{d}\alpha\,\mathrm{d}\Omega \tag{7}$$

where

$$B = 4\pi/\lambda'\sin\frac{\theta}{2}\left\{\sin\frac{\theta}{2}\sin\alpha\cos\Omega - \cos\frac{\theta}{2}\right\} \times \sin\mu\sin\alpha\sin\Omega - \cos\frac{\theta}{2}\cos\mu\cos\alpha \tag{8}$$

and

$$\langle Q\rangle_\eta = \tfrac{1}{8}\{Q_1\sin^2\alpha\cos^2\alpha\sin^2\Omega + 4Q_2(\cos^2\alpha\cos^2\Omega + \sin^2\Omega) + Q_3\sin^2\alpha\cos^2\Omega\} \tag{9}$$

$\langle Q\rangle_\eta$ means the average by integrating over angles, η, and Q_i (i = 1–3) in equation (9) may be given in the forms

$$Q_1 = \{4(2\cos^2 2\omega_0 - 1)(2\langle\cos^2 2\Delta_1\rangle_{\mathrm{av}} - 1) + \tfrac{3}{4}(\langle\cos^2 2\Delta_1\rangle_{\mathrm{av}}\cos^2 2\omega_0 + \langle\sin^2 2\Delta_1\rangle_{\mathrm{av}}\sin^2 2\omega_0) + \tfrac{5}{4}\cos 2\omega_0\langle\cos 2\Delta_1\rangle_{\mathrm{av}}\}f(r_{12}) + \tfrac{5}{4}\cos^2\omega_0\langle\cos 2\Delta_1\rangle_{\mathrm{av}} + \tfrac{3}{4} \tag{10}$$

$$Q_2 = -\tfrac{1}{8}\{(2\langle\cos^2 2\Delta_1\rangle_{\mathrm{av}} - 1)(2\cos^2 2\omega_0 - 1) - 1\}f(r_{12}) \tag{11}$$

$$Q_3 = \tfrac{1}{8}[\{(2\langle\cos^2 2\Delta_1\rangle_{\mathrm{av}} - 1)(2\cos^2 2\omega_0 - 1) - 2\cos 2\omega_0\langle\cos^2\Delta_1\rangle_{\mathrm{av}} + 1\}f(r_{12}) - 2\cos 2\omega_0\langle\cos 2\Delta_1\rangle_{\mathrm{av}} + 2] \tag{12}$$

The function $F(\alpha, \Omega, t)$ was determined to satisfy the

condition where a rectangular phase of an electric field strength is applied to nematic liquid crystalline rods which had been oriented in a shear flow direction perpendicular to an applied electric field. The function $F(\alpha, \Omega, t)$ has been determined to represent orientation of rigid macromolecular chains by one of the co-authors, Matsumoto[22]. Here, if we assume that the assembly of the rigid chains form a liquid crystal rod, the optical axes are, on average, parallel to the rod axis. Hence the average value ω_0 in equations (10)–(12) can be fixed to be zero. This assumption is rigorous on the viewpoints of the profile of the H_v pattern and characteristics of nematic liquid crystals[13]. The function $F(\alpha, \Omega, t)$ of the rod must be satisfied by the same diffusion equation given in a previous paper[8].

$$\frac{\partial F}{\partial t} = \Theta \nabla^2 F - \mathrm{div}(F\omega) \tag{13}$$

In equation (13), F is an abbreviation of $F(\alpha, \Omega, t)$ which is the angular distribution function of an axially symmetric particle with a rotational diffusion coefficient Θ given by kT/ξ, where k is the Boltzmann constant, T is the absolute temperature, and ξ is the rotational frictional coefficient. ω is a velocity angular vector under the action of an external field. Of course, it is a question to employ the simple rotational diffusion equation which is not evident in nematics where the complicated elastic and viscous properties have to be taken into account. However, at present, the introduction of viscoelastic properties into a diffusion equation is extremely difficult in estimating the change in H_v pattern from liquid crystalline rods immersed in shear flow under the action of an electric rectangular pulse. Thus, equation (13) was employed as a crude approximation to represent the orientational behaviour of rods.

According to Demetriades[30], the angular velocity ω is expressed as the sum of the angular velocity ω_H, caused by a hydrodynamic force, and the angular velocity ω_E, caused by an electric force, if the inertia term in the equation of motion is negligible. As discussed by Jeffery[31], the angular velocity ω_H is classified into two components

$$\begin{aligned} \omega_{H\alpha} &= \tfrac{1}{4} GR \sin 2\alpha \sin 2\Omega \\ \omega_{H\Omega} &= \tfrac{1}{2} G(1 + R\cos 2\Omega) \end{aligned} \tag{14}$$

where G is the velocity gradient of flow and R is given by $(P^2 - 1)/(P^2 + 1)$, where P is the axial ratio.

On the other hand, the angular velocity ω_E is also classified into two components

$$\begin{aligned} \omega_{E\alpha} = {} & \frac{1}{\xi}\{\mu' E \cos\alpha \cos\Omega \\ & + (g_{e1} - g_{e2}) E^2 \sin\alpha \cos\alpha \cos^2\Omega\} \\ \omega_{E\Omega} = {} & -\frac{1}{\xi}\left\{\mu' E \frac{\sin\Omega}{\sin\alpha} + (g_{e1} - g_{e2}) E^2 \sin\Omega\cos\Omega\right\} \end{aligned} \tag{15}$$

where μ' is the apparent permanent dipole moment in solution and g_{e1} and g_{e2} are the electric polarizabilities along the symmetry and transverse axes, respectively. E is the electric field strength.

Returning to *Figure 1*, the solution containing ellipsoidal particles is flowing in the X_2 direction and the velocity **u** is expressed as $u = (0, G, 0)$, where G means a constant velocity gradient. When a constant electric field E is suddenly applied to the X_3 direction, E is expressed as $E = (0, 0, E)$. Setting the angles α and Ω within Cartesian coordinate O–$X_1X_2X_3$, equation (13) can be formulated as

$$\begin{aligned} \frac{1}{\Theta}\frac{\partial F}{\partial t} = {} & \frac{\partial}{\partial u}\left\{1 - u^2 \frac{\partial F}{\partial u}\right\} + \frac{1}{1-u^2}\frac{\partial^2 F}{\partial \Omega^2} \\ & + bE\left\{2uF - (1-u^2)\frac{\partial F}{\partial u}\right\} \\ & + 2aE^2\left\{(3u^2 - 1)F - u(1-u^2)\frac{\partial F}{\partial u}\right\} \\ & + \delta\left[\frac{1+R}{2}\left\{\sqrt{1-u^2}\frac{\partial F}{\partial u}\cos\Omega \right.\right. \\ & \left. + \frac{u}{\sqrt{1-u^2}}\sin\Omega\frac{\partial F}{\partial \Omega}\right\} \\ & \left. + R\sqrt{1-u^2}\left\{3uF - (1-u^2)\frac{\partial F}{\partial u}\right\}\cos\Omega\right] \end{aligned} \tag{16}$$

where

$$\delta = \frac{G}{\Theta} \quad b = \frac{\mu'}{kT} \quad a = \frac{g_{e1} - g_{e2}}{2kT} \quad u = \cos\alpha \tag{17}$$

Here it should be noted that the angular distribution function can be expanded into the function series made by the product between power series δ and E and a spherical harmonic as

$$F(\alpha, \Omega, t) = \sum_l \sum_m \sum_p \sum_n K_{lm}^{np} E^n \delta^p P_l^m(u) \cos m\Omega \tag{18}$$

where $P_l^m(u)$ is the associated Legendre function of the lth order and mth degree. After substituting equation (18) into equation (16), we can obtain recurrence relations of K_{lm}^{np} by setting each coefficient of the powers of δ and E as equal to zero, using the property of the orthogonal function. Furthermore, the coefficients K_{lm}^{np} in the build-up process could be calculated by the recurrence relation on the basis of the initial condition in which the solute particles have been arranged under the stationary shear flow before applying an electric field. Actually the coefficients up to the fourth order with respect to δ and E could be determined using the computer software REDUCE. Thus, the final result for the orientation distribution function $F(\alpha, \Omega, t)$ may be given by

$$\begin{aligned} F = {} & K_{00}^{00} P_0^0 + \delta K_{21}^{01} P_2^1 \cos\Omega \\ & + \delta^2[(K_{20}^{02} P_2^0 + K_{40}^{02} P_4^0) + (K_{22}^{02} P_2^2 + K_{42}^{02} P_4^2)\cos 2\Omega] \\ & + \delta^3[(K_{21}^{03} P_2^1 + K_{41}^{03} P_4^1 + K_{61}^{03} P_6^1)\cos\Omega \\ & + (K_{43}^{03} P_4^3 K_{63}^{03} P_6^3)\cos 3\Omega] \\ & + \delta^4[(K_{20}^{04} P_2^0 + K_{40}^{04} P_4^0 + K_{60}^{04} P_6^0 + K_{80}^{04} P_8^0) \\ & + (K_{22}^{04} P_2^2 + K_{42}^{04} P_4^2 + K_{62}^{04} P_6^2 + K_{82}^{04} P_8^2)\cos 2\Omega \\ & + (K_{44}^{04} P_4^4 + K_{64}^{04} P_6^4 + K_{84}^{04} P_8^4)\cos 4\Omega] \\ & + E[K_{10}^{10} P_1^0 + \delta(K_{11}^{11} P_1^1 K_{31}^{11} P_3^1)\cos\Omega \end{aligned}$$

$$+\delta^2\{(K_{10}^{12}P_1^0+K_{30}^{12}P_3^0+K_{50}^{12}P_5^0)$$
$$+(K_{32}^{12}P_3^2+K_{52}^{12}P_5^2)\cos\Omega\}+\cdots]$$
$$+E^2[K_{20}^{20}P_2^0+\delta(K_{21}^{21}P_2^1+K_{41}^{21}P_4^1)\cos\Omega$$
$$+\delta^2\{(K_{20}^{22}P_2^0+K_{40}^{22}P_4^0+K_{60}^{22}P_6^0)$$
$$+(K_{22}^{22}P_2^2+K_{42}^{22}P_4^2+K_{62}^{22}P_6^2)\cos 2\Omega\}+\cdots]$$
$$+E^3[(K_{10}^{30}P_1^0+K_{30}^{30}P_3^0)$$
$$+\delta(K_{11}^{31}P_1^1+K_{31}^{31}P_3^1+K_{51}^{31}P_5^1)\cos\Omega+\cdots]$$
$$+E^4[(K_{20}^{40}P_2^0+K_{40}^{40}P_4^0+\cdots)+\cdots]+\cdots \qquad (19)$$

where K_{lm}^{np} are the expansion coefficients and most terms contain Θt.

The actual calculations were performed up to the fourth order perturbation. The coefficients K_{lm}^{np} are described in the Appendix. Unfortunately some coefficients, K_{80}^{04}, K_{82}^{04}, K_{84}^{04}, K_{42}^{22}, K_{62}^{22}, K_{31}^{31}, K_{51}^{31}, and K_{40}^{40} could not be determined. The terminal error contains the serious unfavourable possibility that $F(\alpha, \Omega, t)$, takes the negative region against angular parts. The exact description up to the higher order coefficients of equation (19) is important in calculating the birefringence and the extinction angle of an axially symmetric macromolecule both with a permanent dipole moment and with an induced dipole moment. The exact formulation causes a much more significant effect on the calculated profiles of small angle light scattering patterns, since the scattered intensity distribution is given by integrating complicated term $F(\alpha, \Omega, t)\langle Q\rangle_\eta \cos Br_{12}$ in equation (7) over a three-dimensional space. To check this problem, numerical calculations of $F(\alpha, \Omega, t)$ were carried out by changing the values of given parameters.

Due to $\omega_0 = 0$, we can employ the same values of b and a in equation (17) which has been measured for poly(γ-benzyl-L-benzyl-L-glutamate) in chloroform, the concentration being about 11 vol%[13]. The values b and a in equation (17) were chosen to be 2.27×10^{-2} and 5.66×10^{-6}, respectively. To justify the values, we shall briefly refer to the experimental procedure. These values were determined as two parameters $\beta(=bE)$ and $\gamma(=aE^2)$ in a molecular orientation distribution function, according to the theory of the steady-state electric birefringence. In doing so, the second order orientation factor $\Phi(\beta, \gamma)$ was determined as $\Delta n/n_s$, based on the E-dependence of birefringence Δn, in which n_s is the steady-state birefringence at infinite field strength. On the other hand, the factor $\Phi(\beta, \gamma)$ at various field strengths with units of $V^2\,cm^{-2}$ was obtained as the second order moments of the molecular orientation function proposed by Holcomb and Tinoco[19]. By using the same method proposed by O'konski *et al.*[16], the theoretical result could be fitted to the experimental one by the proper choice of the relation between β and γ (see Figures 7 and 8 in ref. 13) and consequently, as discussed above, the coefficients $b = (\beta/E)$ and $a = (\gamma/E^2)$ could be determined as 2.27×10^{-2} and 5.16×10^{-6}, respectively, in which the units of β and γ are determined experimentally as $V\,cm^{-1}$ and $V^2\,cm^{-2}$, respectively. The coefficients b and a become zero dimensional order, if E is given by $V\,cm^{-1}$ as discussed in the previous paper[13].

Figure 2 shows the orientation distribution function $\langle F(\alpha, t)\rangle_\Omega$ under a shear flow in the absence of applied electric field ($E = 0\,V\,cm^{-1}$) and the corresponding H_v scattering patterns. The bracket $\langle\,\rangle_\Omega$ means the numerical integration of equation (19) over the angle Ω. The parameter δ in equation (16) indicates the strength of shear flow. At $\delta = 0$, indicating the absence of a shear flow, the rods show a random orientation, while at $\delta = 4$, the function shows a maximum density at $\alpha = 90°$, indicating the preferential orientation of rods with respect to the X_2 axis by a shear flow.

The patterns show X-type at $\delta = 0$, indicating an almost random orientation of rods and the lobes become duller with increasing L/c, i.e., with increasing orientational disorder of the optical axes with respect to the rod axis. Hence, the scattered intensity exhibits an X-type pattern showing a clear μ-dependence when the optical axes are oriented perfectly with respect to the rod axis. By contrast, when the rods (the optical axes being oriented with large orientational fluctuation with respect to the rod axis), are oriented randomly, the scattered intensity tends to be independent of μ, so that the scattering pattern becomes circular[13]. The lobes are extended in the meridional direction at $\delta = 4$, indicating the preferential orientation of rods with respect to the X_2 axis by the shear flow.

Figure 3 shows the orientation function $\langle F(\alpha, t)\rangle_\Omega$ of rods when the electric field is applied to the X_3 axis. The numerical calculations at $\delta = 0.0001$ and $\Theta t = 2$ were

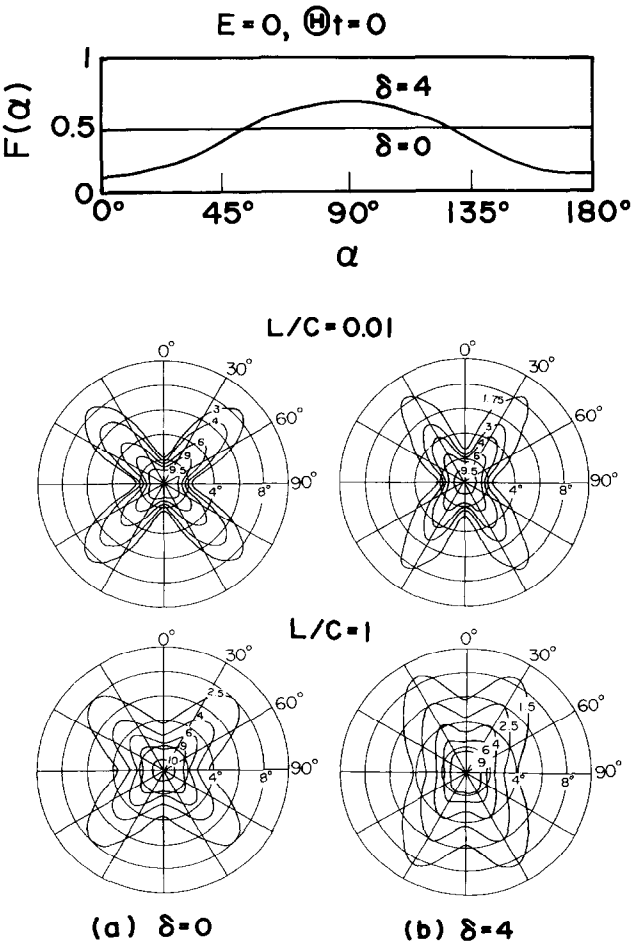

Figure 2 Orientational distribution function of $\langle F(\alpha, t)\rangle_\Omega$ at $\delta = 0$ and 4 in the absence of an electric field and the corresponding H_v light scattering patterns

carried out for three kinds of expansions of $\langle F(\alpha, t)\rangle_\Omega$ in a series of E [see equation (19)]; (i) the bracket [ ] of E^3 (the third order) and that of E^4 (the fourth order) terms are zero, (ii) the bracket of E^3 term is not zero but that of E^4 is zero, and (iii) the brackets of E^3 and E^4 terms are not zero. At $E = 50\,\mathrm{V\,cm^{-1}}$, all the functions $\langle F(\alpha, t)\rangle_\Omega$ calculated by the three cases exhibit similar profile and take positive values over the whole angle of α. At $E = 100\,\mathrm{V\,cm^{-1}}$, the function of $\langle F(\alpha, t)\rangle_\Omega$ takes positive value over the whole angle of α in case (i), while the functions calculated by cases (ii) and (iii) tend to be negative as α becomes wider. The function calculated by using case (i) tends to increase gradually at $\alpha > 90°$, which is different from the tendency at $E = 50\,\mathrm{V\,cm^{-1}}$. Judging from the profiles at $E = 50\,\mathrm{V\,cm^{-1}}$, this small duller increase is probably attributed to a periodic noise

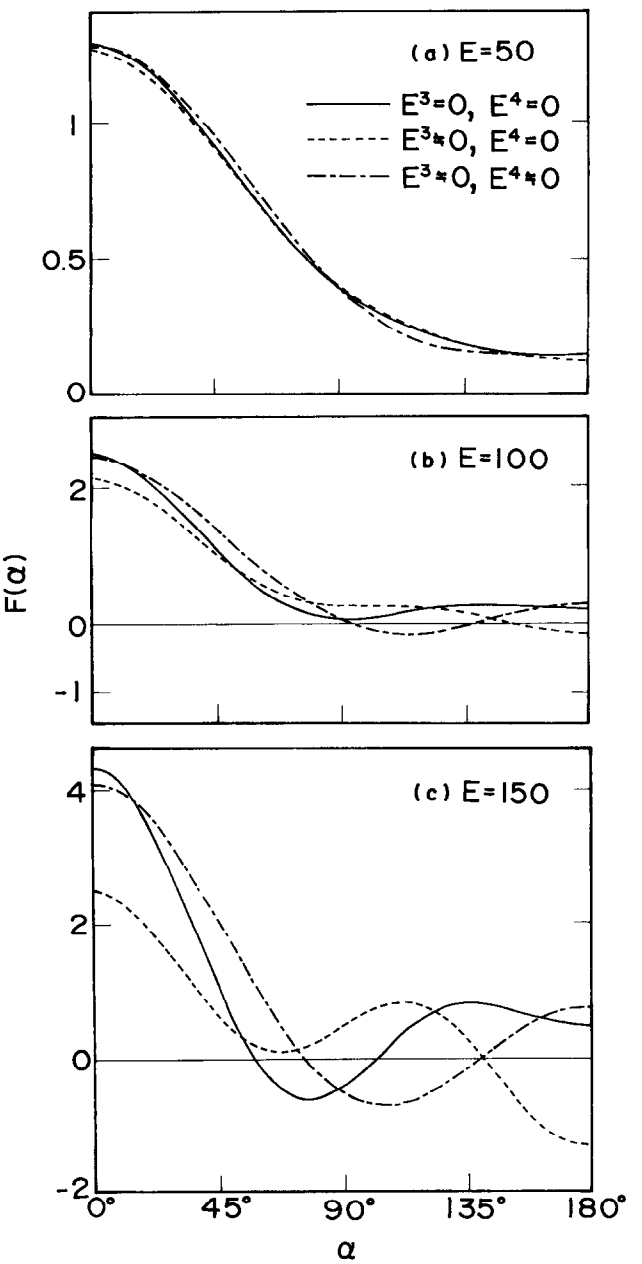

Figure 3 Orientational distribution function of $\langle F(\alpha, t)\rangle_\Omega$ at $\delta = 0.0001$ and $\Theta t = 2$ at electric fields of $E = 50$, 100 and $150\,\mathrm{V\,cm^{-1}}$, calculated by three cases; (i) $E^3 = 0$ and $E^4 = 0$, (ii) $E^3 = 0$ and $E^4 \neq 0$, and (iii) $E^3 \neq 0$ and $E^4 \neq 0$

leading to terminal error of a series of expansion of the function. Similar periodic noise was also observed for case (iii). On the other hand, the function calculated by using case (ii) shows a rather simple decreasing curve similar to the profiles of the curves calculated at $E = 50\,\mathrm{V\,cm^{-1}}$, although it takes negative values at $\alpha > 140°$. At $E = 150\,\mathrm{V\,cm^{-1}}$, all the functions calculated by the three cases show considerable periodic noise having negative part. As described before the increase in periodic noise is attributed to the terminal error due to the difficulty in determining the fourth moment coefficients. Judging from the curve profiles, the following calculations were carried out using case (ii) at $E = 100\,\mathrm{V\,cm^{-1}}$, since the change in H_v light scattering patterns calculated at lower electric field strength such as $E = 50\,\mathrm{V\,cm^{-1}}$ is not so effective to the change in parameters δ and Θt.

To support the justification of numerical calculations by case (ii), based on another background, the numerical calculations of transient electric birefringence were carried out for three cases (i), (ii), and (iii), using a matrix with nine components, as

$$n^2 = \begin{vmatrix} n_{11}^2 & n_{12}^2 & n_{13}^2 \\ n_{21}^2 & n_{22}^2 & n_{23}^2 \\ n_{31}^2 & n_{32}^2 & n_{33}^2 \end{vmatrix} \tag{20}$$

Accordingly, the birefringence Δ is given by[32]

$$\Delta \doteqdot \frac{1}{2n}\left[(n_{33}^2 - n_{11}^2)^2 + (2n_{31}^2)^2\right]^{1/2} \tag{21}$$

where n corresponds to $(n_{11} + n_{33})/2$ and the components n_{33}, n_{11}, and n_{31} are represented by using the angular distribution function $F(\alpha, \Omega, t)$ as

$$n_{33}^2 = n_0^2 + 4\pi C_v\left\{g_{e2} + (g_{e1} - g_{e2}) \times \int_0^{2\pi}\int_0^{\pi} \cos^2\alpha\, F(\alpha, \Omega, t)\sin\alpha\, d\alpha\, d\Omega\right\} \tag{22}$$

$$n_{11}^2 = n_0^2 + 4\pi C_v\left\{g_{e2} + (g_{e1} - g_{e2}) \times \int_0^{2\pi}\int_0^{\pi} \sin^2\alpha\frac{1 + \cos 2\Omega}{2} \times F(\alpha, \Omega, t)\sin\alpha\, d\alpha\, d\Omega\right\} \tag{23}$$

and

$$n_{31}^2 = 4\pi C_v(g_{e1} - g_{e2})\int_0^{2\pi}\int_0^{\pi} \cos\alpha\sin\alpha \times F(\alpha, \Omega, t)\cos\Omega\sin\alpha\, d\alpha\, d\Omega \tag{24}$$

where C_v is the volume concentration. In actual calculation, it may be assumed that the molecular chains are perfectly oriented parallel to the rod axis.

To check the increasing behaviour of Δ with Θt, the birefringence Δ is normalized as

$$Y(t) = \frac{\Delta - \Delta_{E=0}}{\Delta_{t\to\infty} - \Delta_{E=0}} \tag{25}$$

where $\Delta_{E=0}$ is the initial birefringence at $E = 0$ and $\Delta_{t\to\infty}$ is the birefringence at the steady-state after applying the electric field. The terms $-\Delta_{E=0}$ in a numerator and a denominator of equation (25) are

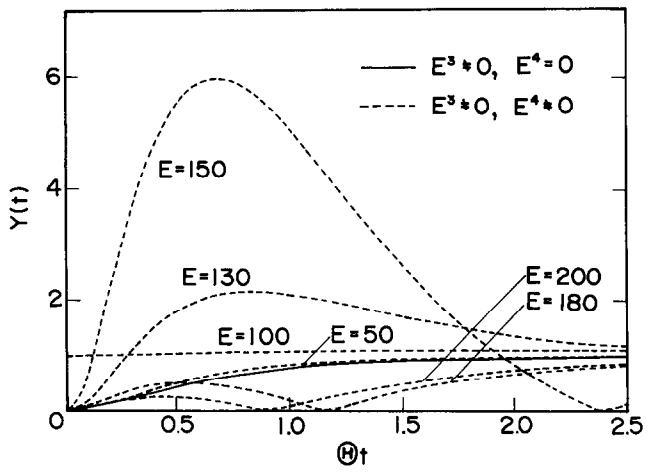

Figure 4 Normalized electric birefringence $Y(t)$ against Θt, calculated by cases (ii) and (iii) at the indicated value of E

introduced to eliminate birefringence by a shear flow effect. Therefore, it is evident that the value of normalized birefringence, $Y(t)$, increases monotonically with increasing Θt and becomes unity at $\Theta t \rightarrow \infty$.

Figure 4 shows the results calculated as a function of E in cases (ii) and (iii). At a fixed value of Θt, the value calculated by case (ii) was confirmed to be slightly larger with increasing E. The difference, however, is very small and all the calculated values are almost independent of E. Thus the behaviour is represented as a thin solid curve. This tendency is obviously rigorous, since $Y(t)$ at each value of E is independent of a shear flow effect.

In contrast, the dotted curves calculated by using case (iii) show different profiles except the curves at $E = 50\,\mathrm{V\,cm^{-1}}$. All curves show increasing behaviour at earlier time scale and they tend to decrease beyond their maximum value. Among them, the curves at $E = 180$ and $200\,\mathrm{V\,cm^{-1}}$ show negative value and tend to increase again. Anyway, the behaviour showing overshoot is in contradiction to the monotonical rise birefringence, since a shear flow effect is eliminated in equation (25). Thus the monotonical rise curves support the calculation of H_v patterns by using case (ii) at $E = 100\,\mathrm{V\,cm^{-1}}$. Incidentally, the good agreement between cases (ii) and (iii) at $E = 50\,\mathrm{V\,cm^{-1}}$ is probably thought to be due to the fact that the terminal error of the coefficients associated with E^3 and E^4 does not provide any serious effect on the orientation distribution function $F(\alpha, \Omega, t)$.

Figure 5 shows the orientation function of $\langle F(\alpha, t)\rangle_\Omega$ in an instantaneous state ($\Theta t = 0$) of an applied electric field of $100\,\mathrm{V\,cm^{-1}}$ at $\delta = 4$ and the corresponding H_v patterns given as a function of L/c. The orientation function has two maximum peaks at $\alpha = 0°$ (180°) and 90°. The higher peak at $\alpha = 0°$ (180°) is related to the applied electric field and lower peak at $\alpha = 90°$, indicating the shear flow as observed in *Figure 2*. The lobes showing clear μ-dependence in the H_v pattern are extended in the horizontal direction at wider scattering angle, reflecting the large peak of $\langle F(\alpha, t)\rangle_\Omega$ at $\alpha = 0°$. Close observation reveals that in addition to the four lobes discussed above, there exist another small four lobes at $L/c = 0.01$ extended in the vertical direction reflecting the small peak of $\langle F(\alpha, t)\rangle_\Omega$ at $\alpha = 90°$. The appearance of the small lobes becomes clearer with increasing L/c and at $L/c = 1$, the small four lobes are

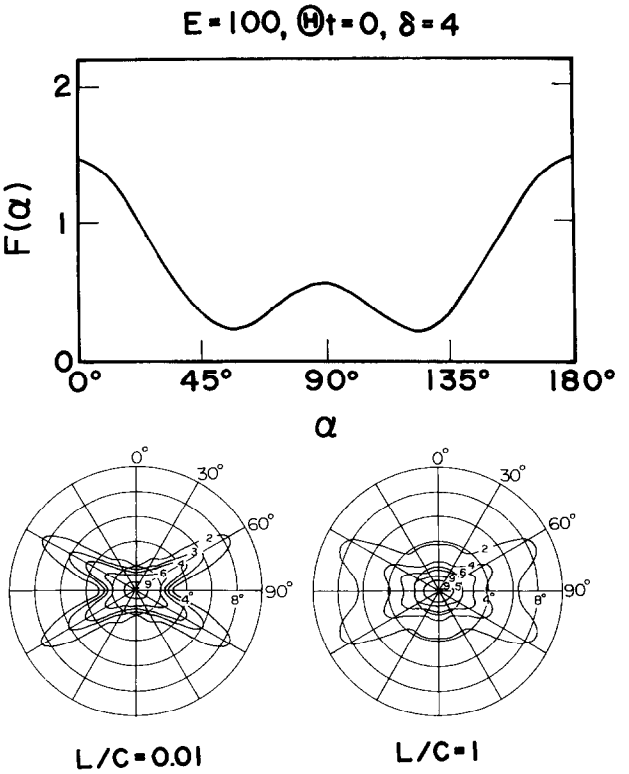

Figure 5 Orientational distribution function of $\langle F(\alpha, t)\rangle_\Omega$ at $\delta = 4$ and $\Theta t = 0$ in the absence of an electric field and the corresponding H_v light scattering patterns at $L/c = 0.01$ and 1

amalgamated into two lobes along the vertical direction. Incidentally, the patterns with eight lobes have already been observed for H_v scattering from drawn nylon 6 films. However, we have had no idea of how to pursue mathematical analysis because of the difficulty in obtaining a suitable orientation distribution function to represent complicated orientation behaviour of rods with the nylon 6 under uniaxial stretching[23,24]. Judging from the two patterns in *Figure 5*, it is found that even in uniaxial elongation, the orientation behaviour of rods with the drawn nylon 6 film deviates from the uniaxial mode.

Figure 6 shows H_v scattering patterns at $L/c = 0.01$ and 1 with increasing Θt, when the parameters E and δ are fixed to be 100 and 0.0001, respectively. The lobes are extended in the vertical direction in the absence of applied field, because of the steady-state flow in the X_2 direction in *Figure 1*. With increasing time, the lobes are extended in the horizontal direction, reflecting the applied electric field in the X_3 direction. The function to calculate the H_v patterns at $\Theta t = 2$ corresponds to the dotted curve by case (ii) in *Figure 3*. Fortunately, the small negative part of the function at $\alpha > 140°$ shown in *Figure 3b* did not influence unfavourable effects on the calculated patterns.

Here it should be noted that the H_v patterns show normal profile which has been calculated by using the function with the symmetrical relationship $\langle F(\alpha, t)\rangle_\Omega = \langle F(\pi - \alpha, t)\rangle_\Omega$, although the function used for the calculation of H_v patterns does not satisfy the above relationship but only satisfies the relationship $\langle F(\alpha, t)\rangle_\Omega = \langle F(2\pi - \alpha, t)\rangle_\Omega$. Such an abnormal phenomenon is due to the fact that equation (19) means the orientation function of one end (head) of the rod and

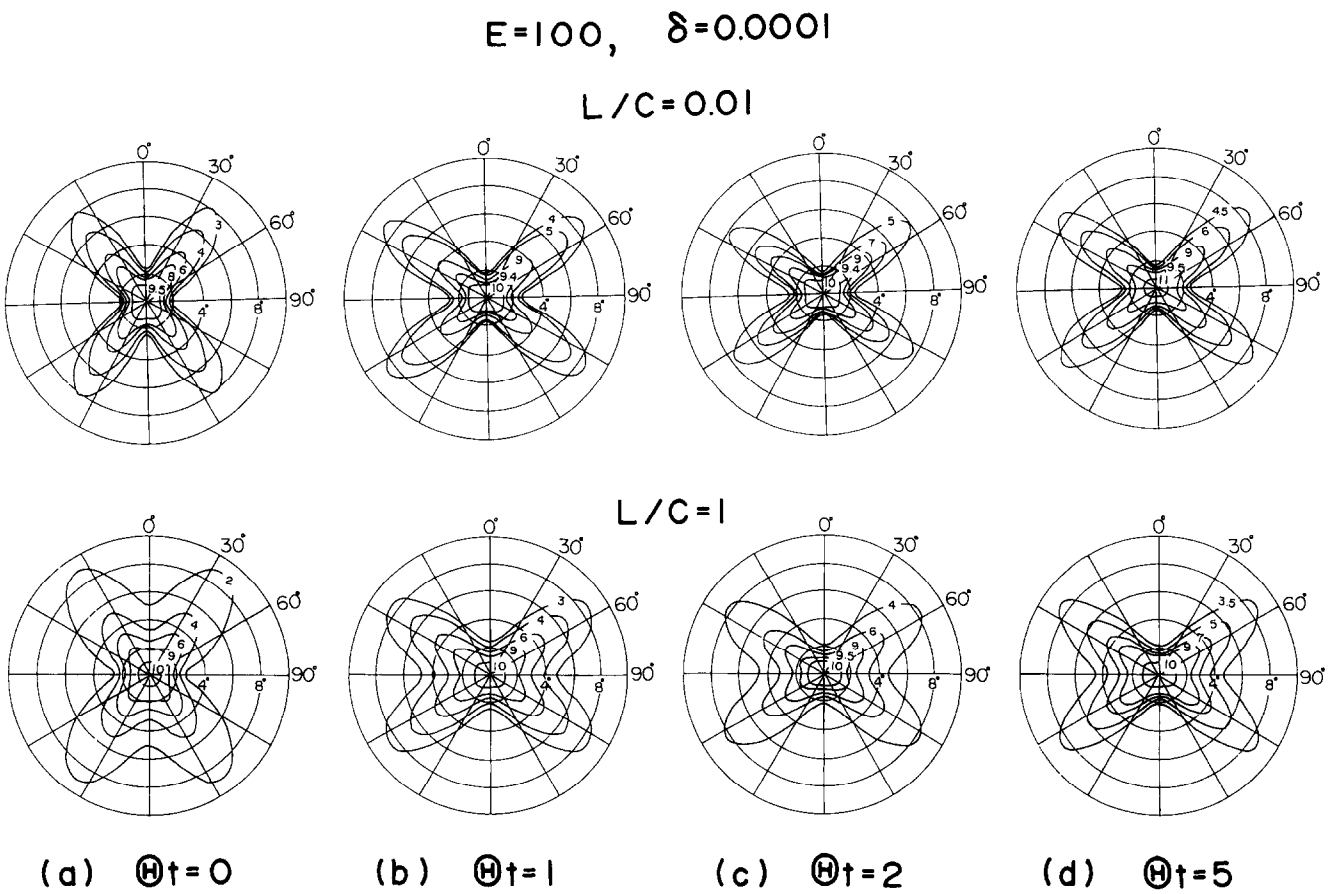

Figure 6 Change of H_v light scattering patterns with increasing Θt, calculated at $\delta = 0.0001$ and $E = 100\,\mathrm{V\,cm^{-1}}$

inevitably the function becomes lowest at = 180°, while the calculated patterns cannot recognize both ends (head and tail) of a rod, consistent with the results observed by optical instrument. This indicates that in the calculation process of H_v light scattering patterns, the terms containing $P_l^m(x)(l$: odd) become zero by integrating over a three-dimensional space and the calculated patterns show rigorous profile in good agreement with those observed. Thus, it is unnecessary to consider the symmetry of the orientation function obtained as a series expansion of polar and azimuthal angles on calculating light scattering patterns under polarization condition.

To study the advantage of polarized light scattering in estimating orientational behaviour of rods and of optical axes in comparison with other optical quantities, the second and fourth order orientation factors have been proposed[33,34]. That is, if molecular chains are oriented parallel to the rod axis without the orientational fluctuation, the orientation factors of molecular chains for the present system can be defined by

$$F_{lm} = \langle P_l^m(\cos\alpha)\cos m\Omega\rangle = \int_0^{2\pi}\int_0^{\pi} f(\alpha, \Omega, t)P_l^m(\cos\alpha) \times \cos m\Omega \sin\alpha\, d\alpha\, d\Omega \quad (26)$$

where l and m are integers and $f(\alpha, \Omega, t)$ is the normalized function of $F(\alpha, \Omega, t)$ given by

$$f(\alpha, \Omega, t) = \frac{F(\alpha, \Omega, t)}{\int_0^{2\pi}\int_0^{\pi} F(\alpha, \Omega, t)\sin\alpha\, d\alpha\, d\Omega} \quad (27)$$

The electric birefringence given in equation (21) contains the information of the second-order orientation factors, F_{20}, F_{21}, and F_{22}. Generally, for industrial materials such as calender films and inflation films taking biaxial orientation, the orientation factors, F_{20} and F_{22} can be evaluated by birefringence and dye dichroism measurements[33] and F_{40}, F_{42}, and F_{44} can be evaluated by fluorescence polarization dichroism[34]. Of course, for crystalline polymer, the higher order factors F_{lm} (l: even and m: even) beyond 6 can be estimated from crystal orientation distribution function obtained by X-ray diffraction[35]. However, the factors F_{lm} (l: even and m: odd or even) become zero because of orthogonal biaxial symmetry of the orientation distribution function for most of the industrial products such as $f(\pm\cos\alpha, \pm\Omega) = f(\pm\cos\alpha, \pi \pm \Omega)$.

Figure 7 shows change in the orientation factor F_{20} with increasing Θt and *Figure 8* shows all the factors up to the fourth order except F_{20}. The calculations were carried out at $\delta = 0.0001$ and $E = 100\,\mathrm{V\,cm^{-1}}$. F_{20} characterizes the orientation distribution of molecular chains with variation between $-1/2$ and 1. For random orientation, F_{20} is zero, while for complete orientation parallel and perpendicular to the X_3 axis in *Figure 1*, F_{20} are 1 and $-1/2$, respectively. Before applying the rectangular electric pulse, F_{20} takes negative values indicating the preferential orientation perpendicular to the X_3 axis because of the influence of shear flow, but tends to increase indicating the preferential orientation to the X_3 axis by the influence of the electric field. The value tends to level off with further increase in Θt beyond 3. It is seen that the other factors shown in *Figure 8* are

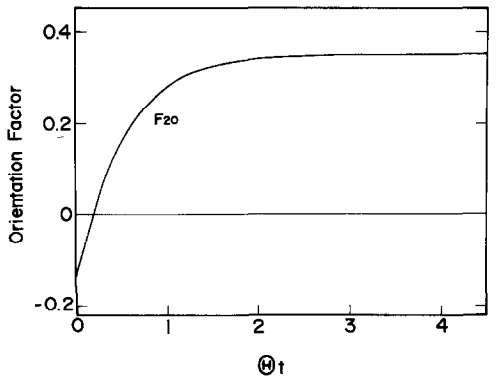

Figure 7 The second order orientation factor F_{20} against Θt, calculated at $\delta = 0.0001$ and $E = 100\,\mathrm{V\,cm^{-1}}$

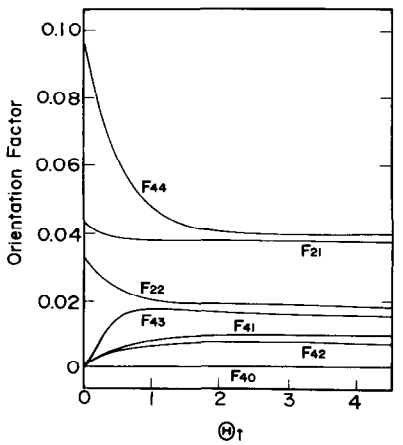

Figure 8 The first, second, third, and fourth order orientation factors F_{21}, F_{22}, F_{40}, F_{41}, F_{42}, F_{43}, and F_{44} using the same values of δ and E used in *Figure 7*

less effective for change of molecular orientation rather than F_{20}. This means that electric birefringence is strongly affected by F_{20} and is hardly affected by F_{21} and F_{22}.

Here it should be noted that the birefringence gives the second order orientation factors, and these factors cannot represent the detailed orientation behaviour of molecules. Thus, nobody can infer the complicated orientation function shown in *Figure 5* from the second-order orientation factors. Namely, it is evident that the same values of the factors can be realized easily from another monotonous curve. Nevertheless, the orientation of rigid molecules under an electric field and/or a shear flow have been estimated mainly by birefringence measurements[15–22]. For polarized light scattering, the scattered intensity is related to the orientation distribution functions of rods in terms of high order moments and the profile of scattering pattern reflects the complicated orientation of rods sensitively as shown in the patterns in *Figure 5*. Accordingly, small angle light scattering has an advantage in studying the detailed orientation behaviour of superstructures such as spherulitic and rod-like textures in comparison with birefringence.

CONCLUSION

The theoretical analysis of light scattering patterns was carried out when an electric field was applied to the liquid crystal rods immersed in shear flow in order to study the change of pattern in complicated oriented systems. The orientation distribution function of the rod axis was assured to be equal to the rotational diffusion equation for rotational ellipsoidal particles in solution. The equation was approximately solved when the solute particles oriented by a shear flow were acted on by a rectangular electric pulse along the direction of the velocity gradient of flow. In actual calculation of H_v scattering patterns, the orientation of optical axes with respect to the rod axis was assumed to be dependent upon the position within a rod.

The H_v patterns exhibited scattering lobes extended in the meridional direction indicating the preferential orientation in the shear flow direction in the absence of applied electric field. When a rectangular pulse was applied to the direction perpendicular to the shear flow the scattering pattern at the initial stage showed eight lobes, in which the four lobes in the horizontal direction show clear μ-dependence but the four remaining small lobes in the vertical direction were unclear. The former lobes were associated with the preferential orientation of rods in the direction of an applied electric field and the latter, in the direction of a shear flow. With increasing time, the four scattering lobes simply tend to be extended in the horizontal direction. This indicates that polarized light scattering reflect the complicated orientational behaviour of rods sensitively, in comparison with birefringence reflecting only the second order moment of the distribution function[22].

REFERENCES

1 Clough, S. B., van Aartsen, J. J. and Stein, R. S. *J. Appl. Phys.* 1965, **36**, 3072
2 Rhodes, M. B. and Stein, R. S. *J. Polym. Sci. A-2*, 1969, **7**, 1538
3 Sawatari, C., Murakami, T. and Matsuo, M. *Polym. J.* 1983, **15**, 33
4 Matsuo, M., Tamada, M., Terada, T., Sawatari, C. and Niwa, M. *Macromolecules* 1982, **15**, 998
5 Sawatari, C., Iida, M. and Matsuo, M. *Macromolecules* 1984, **17**, 1765
6 Clough, S. B., van Aartsen, J. J. and Stein R. S. *J. Appl. Phys.* 1965, **36**, 3072
7 Hayashi, N., Murakami, Y., Moritani, M., Hashimoto, T. and Kawai, H. *Polym. J.* 1973, **4**, 560
8 Matsuo, M., Kakei, K. and Nagaoka, Y. *J. Chem. Phys.* 1981, **75**, 5925
9 Wilkers, G. L. *Mol. Cryst. Liq. Cryst.* 1972, **18**, 65
10 Iizuka, E., Keira, T. and Wada, A. *Mol. Cryst. Liq. Cryst.* 1973, **23**, 13
11 Matsuo, M., Ozaki, F., Konno, Y. and Ogita, T. *J. Polym. Sci., Polym. Phys. Ed.* 1981, **19**, 1531
12 Ozaki, F., Ogita, T. and Matsuo, M. *Macromolecules* 1981, **14**, 299
13 Matsuo, M., Kakei, K., Nagaoka, Y., Ozaki, F., Murai, M. and Ogita, T. *J. Chem. Phys.* 1981, **75**, 5911
14 Matsuo, M., Kakei, K., Ozaki, F. and Ogita, T. *J. Chem. Phys.* 1982, **76**, 3974
15 O'konski, C. T. and Haltner, A. J. *J. Am. Chem. Soc.* 1957, **79**, 5634
16 O'konski, C. T., Yoshikawa, K. and Orttung, W. H. *J. Phys. Chem.* 1959, **63**, 1558
17 Shah, M., Thompson, D. C. and Hart, C. M. *J. Phys. Chem.* 1963, **67**, 1170
18 Shah, M. *J. Phys. Chem.* 1963, **67**, 2215
19 Holcomb, D. N. and Tinoco Jr., I. *J. Phys. Chem.* 1963, **67**, 2691
20 Benoit, H. *Ann. Phys. (Leipzig)* 1951, **6**, 561
21 Matsumoto, M., Watanabe, H. and Yoshioka, K. *J. Phys. Chem.* 1970, **74**, 2182

22 Matsumoto, M. *J. Chem. Phys.* 1992, **96**, 4750
23 Matsuo, M., Hattori, H., Nomura, S. and Kawai, H. *J. Polym. Sci. Polym. Phys. Ed.* 1976, **14**, 223
24 Matsuo, M., Seino, Y., Watanabe, T., Moriguchi, S., Ozaki, F. and Ogita, T. *Polym. J.* 1981, **13**, 755
25 For example, Caesar, G. P., Levenson, R. A. and Gray, H. B. *J. Am. Chem. Soc.* 1969, **91**, 772
26 Matso, M., Sakai, Y., Maeda, E., Hara, C., Iida, M. and Manley, R. St. J. *J. Phys. Chem.* 1994, **98**, 10988
27 van de Halst, H. C. 'Light Scattering by Small Particles', Wiley, New York, 1951
28 Stein, R. S. and Chu, W. *J. Polym. Sci. A-2* 1970, **8**, 1137
29 Hashimoto, T., Murakami, Y. and Kawai, H. *J. Polym. Sci. Polym. Phys. Ed.* 1975, **13**, 1613
30 Demetriades, T. *J. Chem. Phys.* 1958, **29**, 1054
31 Jeffery, G. B. *Proc. R. Soc. London, Ser. A* 1922, **102**, 161
32 Peterlin, A. and Stuart, H. A. *Z. Phys.* 1939, **112**, 129
33 Nomura, S., Kawai, H., Kimura, I. and Kaziyama, M. *J. Polym. Sci. A-2* 1967, **5**, 479
34 Kimura, I., Kaziyama, M., Nomura, S. and Kawai, H. *J. Polym. Sci. A-2* 1969, **7**, 709
35 Roe, R. J. and Krigbaum, W. R. *J. Chem. Phys.* 1964, **40**, 2608

APPENDIX

The coefficients in equation (19) which did not appear in the previous paper are described as

$$K_{40}^{02} = -\frac{1}{4\pi}\frac{1}{70}R^2$$

$$K_{42}^{02} = \frac{1}{4\pi}\frac{1}{840}R^2$$

$$K_{41}^{03} = \frac{1}{4\pi}\frac{1}{600}R^2\left(\frac{15}{308}R-1\right)$$

$$K_{43}^{03} = \frac{1}{4\pi}\frac{1}{25\,200}R^2\left(\frac{15}{44}R+1\right)$$

$$K_{61}^{03} = -\frac{1}{4\pi}\frac{1}{5544}R^3$$

$$K_{63}^{03} = \frac{1}{4\pi}\frac{1}{332\,640}R^3$$

$$K_{10}^{12} = \frac{1}{4\pi}b\left[\frac{1}{4}\left(\frac{1}{105}R^2+\frac{1}{12}R-\frac{1}{4}\right)-\left\{\frac{1}{2}\left(\frac{101}{26\,250}R^2+\frac{1}{24}R-\frac{1}{8}\right)+\left(\frac{41}{3500}R^2+\frac{1}{40}-\frac{1}{8}\right)\Theta t+\frac{1}{8}\left(\frac{9}{25}R^2-1\right)\Theta^2t^2\right\}\exp(-2\Theta t)-\frac{2}{4375}R^2\exp(-12\Theta t)\right]$$

$$K_{30}^{12} = \frac{1}{4\pi}bR\left[\frac{1}{24}\left(\frac{1}{15}R+1\right)-\frac{1}{25}\left\{\frac{4}{5}\left(\frac{17}{120}R+1\right)+\left(\frac{3}{5}R+1\right)\Theta t\right\}\exp(-2\Theta t)+\frac{1}{25}\left\{\frac{1}{120}\left(\frac{79}{15}R-29\right)+\left(\frac{1}{15}R-1\right)\Theta t\right\}\times\exp(-12\Theta t)\right]$$

$$K_{32}^{12} = \frac{1}{24\pi}bR\left[\frac{1}{36}\left(\frac{3}{10}R+1\right)-\frac{1}{25}\left\{\frac{3}{5}\left(\frac{3}{10}R+1\right)+\left(\frac{3}{5}R+1\right)\Theta t\right\}\exp\left(-2\Theta t\right)-\frac{1}{50}\left\{\frac{17}{90}\left(\frac{3}{10}R+1\right)+\left(\frac{1}{5}R+1\right)\Theta t\right\}\exp\left(-2\Theta t\right)\right]$$

$$K_{10}^{10} = \frac{1}{4\pi}b\{1-\exp(-2\Theta t)\}$$

$$K_{11}^{11} = \frac{1}{4\pi}\frac{1}{4}b\left\{\left(\frac{2}{5}R+1\right)-\left\{\left(\frac{2}{5}R+1\right)+2\left(\frac{3}{5}R+1\right)\Theta t\right\}\exp\left(-2\Theta t\right)\right\}$$

$$K_{31}^{11} = \frac{1}{4\pi}\frac{1}{15}bR\left\{1-\frac{4}{5}\exp\left(-2\Theta t\right)-\frac{1}{5}\exp\left(-12\Theta t\right)\right\}$$

$$K_{50}^{12} = -\frac{1}{4\pi}\frac{1}{126}bR^2\left\{1-\frac{24}{35}\exp\left(-2\Theta t\right)-\frac{4}{15}\exp\left(-12\Theta t\right)-\frac{1}{21}\exp\left(-30\Theta t\right)\right\}$$

$$K_{52}^{12} = \frac{1}{4\pi}\frac{1}{2520}bR^2\left\{1-\frac{24}{35}\exp\left(-2\Theta t\right)-\frac{4}{15}\exp(-12\Theta t)-\frac{1}{21}\exp\left(-30\Theta t\right)\right\}$$

$$K_{11}^{13} = \frac{1}{4\pi}b\left[\left\{\frac{1}{1000}R^3\left(-\frac{9}{2}\Theta^3t^3+\frac{69}{70}\Theta^2t^2+\frac{21}{25}\Theta t+\frac{601}{2625}\right)-\frac{1}{400}R^2\left(3\Theta^3t^3+\frac{59}{70}\Theta^2t^2+\frac{437}{1050}\Theta t+\frac{317}{3500}\right)+\frac{1}{40}R\left(\frac{1}{2}\Theta^3t^3+\frac{1}{2}\Theta^2t^2+\frac{1}{3}\Theta t+\frac{1}{9}\right)+\frac{1}{16}\left(\frac{1}{3}\Theta^3t^3+\frac{1}{2}\Theta^2t^2+\frac{1}{2}\Theta t+\frac{1}{4}\right)\right\}\exp\left(-2\Theta t\right)-\left\{\frac{1}{5^4}R^3\left(\frac{3}{140}\Theta t-\frac{1}{139}\right)+\frac{1}{17\,500}R^2(11\Theta t+\frac{557}{180})\right\}\exp\left(-12\Theta t\right)-\frac{1}{8}\left(\frac{1}{525}R^3+\frac{1}{2520}R^2+\frac{1}{45}R+\frac{1}{8}\right)\right]$$

$$K_{41}^{21} = \frac{1}{4\pi}\frac{1}{70}R\left\{\left(b^2+2a\right)-\frac{23}{18}b^2\exp\left(-2\Theta t\right)+\frac{5}{14}\left(b^2-4a\right)\exp(-6\Theta t)-\frac{1}{4}b^2\exp\left(-12\Theta t\right)+\frac{43}{252}\left(b^2-\frac{144}{43}a\right)\exp\left(-20\Theta t\right)\right\}$$

$$K_{22}^{22} = \frac{1}{4\pi}\frac{1}{12^3}\left[\left\{b^2\left(\frac{17}{21}R+5\right)+4a\left(\frac{3}{7}R+1\right)\right\}+\frac{27}{2}b^2\left\{\frac{1}{2}\left(\frac{3866}{70\,875}R^2+\frac{3}{35}R-1\right)-\left(\frac{13}{175}R^2+\frac{76}{105}R+1\right)\Theta t\right\}\exp\left(-2\Theta t\right)-2\left\{\frac{1}{8}b^2\left(\frac{3658}{2401}R^2+\frac{13}{3}R-7\right)+2a\left(\frac{48}{2401}R^2+\frac{3}{7}R+1\right)+\frac{3}{4}b^2\left(\frac{71}{343}R^2-\frac{10}{7}R-7\right)\Theta t+12a\left(\frac{82}{343}R^2+\frac{5}{7}R+1\right)\Theta t-9\left(\frac{3}{7}R+1\right)\left(\frac{1}{7}R+1\right)\left(b^2-4a\right)\Theta^2t^2\right\}\exp(-6\Theta t)+\frac{48}{35}b^2R\left\{\frac{2}{9}\left(\frac{3}{25}R-1\right)-\left(\frac{1}{5}R+1\right)\Theta t\right\}\exp\left(-12\Theta t\right)-\frac{4}{2401}R^2\left(\frac{43}{3}b^2-48a\right)\exp\left(-20\Theta t\right)\right]$$

$$K_{10}^{30} = \frac{1}{4\pi}\frac{1}{15}b\left(b^2-4a\right)\left\{1-\frac{3}{4}\left(1+4\Theta t\right)\exp(-2\Theta t)-\frac{1}{4}\exp\left(-6\Theta t\right)\right\}$$

$$K_{30}^{30} = \frac{1}{4\pi}\frac{1}{15}b\left\{\left(b^2+6a\right)-\frac{3}{5}\left(3b^2+8a\right)\exp(-2\Theta t)+\frac{1}{4}\left(b^2-4a\right)\exp(-6\Theta t)-\frac{1}{5}\left(b^2-14a\right)\exp(-12\Theta t)\right\}$$

$$K_{11}^{31} = \frac{1}{4\pi} b\left[\left\{\tfrac{1}{400} b^2 R\left(21\Theta^2 t^2 + \tfrac{13}{70}\Theta t + \tfrac{1009}{200}\right)\right.\right.$$
$$+ \tfrac{1}{80} b^2\left(7\Theta^2 t^2 + \tfrac{13}{2}\Theta t + \tfrac{21}{8}\right)$$
$$\left.\left. - \tfrac{1}{50} aR\left(3\Theta^2 t^2 + \tfrac{19}{35}\Theta t + \tfrac{949}{1400}\right) - \tfrac{1}{10} a\left(\Theta^2 t^2 - \tfrac{1}{8}\right)\right\}\right.$$
$$\times \exp(-2\Theta t) + \left\{\tfrac{1}{560} b^2 R\left(\Theta t - \tfrac{41}{24}\right) + \tfrac{1}{80} b^2\left(\Theta t + \tfrac{3}{8}\right)\right.$$
$$- \tfrac{1}{140} aR\left(\Theta t - \tfrac{11}{12}\right) - \tfrac{1}{20} a\left(\Theta t + \tfrac{1}{4}\right)\Big\} \exp(-6\Theta t)$$
$$- \tfrac{1}{4375}\left(\tfrac{1}{6} b^2 R - 11aR\right) \exp(-12\Theta t)$$
$$\left. - \tfrac{1}{5}\left(\tfrac{1}{21} b^2 R + \tfrac{3}{16} b^2 - \tfrac{1}{21} aR\right)\right]$$